International Journal of Fatigue 57 (2013) 28–36

Contents lists available at SciVerse ScienceDirect

International Journal of Fatigue

journal homepage: www.elsevier.com/locate/ijfatigue

# A microstructural based understanding of hydrogen-enhanced fatigue of stainless steels

M.L. Martin [a,d], P. Sofronis [b,d], I.M. Robertson [a,d,*], T. Awane [c,d], Y. Murakami [c,d]

[a] Dept. of Materials Science and Engineering, University of Illinois, Urbana, IL 61801, United States
[b] Dept. of Mechanical Science and Engineering, University of Illinois, Urbana, IL 61801, United States
[c] Research Center for Hydrogen Industrial Use and Storage (HYDROGENIUS), National Institute of Advanced Industrial Science and Technology (AIST), Fukuoka, 819-0395 Japan
[d] Inter. Institute for Carbon Neutral Energy Research (WPI-I$^2$CNER), Kyushu University, 744 Moto-oka, Nishi-ku, Fukuoka 819-0395, Japan

ARTICLE INFO

*Article history:*
Received 2 March 2012
Received in revised form 21 August 2012
Accepted 22 August 2012
Available online 9 September 2012

*Keywords:*
Fatigue
Hydrogen
Microstructure
Electron microscopy
Focused-ion beam

ABSTRACT

The microstructure immediately beneath the fracture surface produced during fully-reversed fatigue loading of uncharged and hydrogen-charged 304 and 316 stainless steels has been investigated by using focused ion beam machining in conjunction with transmission electron microscopy. The microstructure beneath striations on the fracture surface is dependent on the presence/absence of hydrogen and varies as a function of distance from the surface. The underlying microstructure also is dependent on the morphology of the fracture surface and is distinctly different beneath striations and flat regions. The differences in evolved microstructure are considered in terms of mechanisms by which hydrogen modifies deformation processes.



## 1. Introduction

With the prospect of transitioning to a hydrogen-based economy, many engineering components (tanks, valves and pipes) will be exposed to high-pressure gaseous hydrogen environments. Consequently, there is a need to understand, both from an engineering and from a fundamental perspective, how high pressure (up to 35 MPa) gaseous hydrogen environments influence the mechanical properties of materials, especially fatigue behavior. Hydrogen is known to embrittle most metals [1,2] and it is found to decrease the fatigue life of steels [3–16]. Specifically for 304 and 316 stainless steels, Murakami et al. [7] have shown a decrease in fatigue lifetime when these steels contain hydrogen concentrations between ~5 and ~47 wt. ppm for 304 and ~2 and ~15 wt. ppm for 316. The microstructure observed in interrupted fatigue tests of 304 stainless steel exhibited a decreasing amount of strain-induced $\alpha'$ martensite with increasing hydrogen concentration [7]. Matsunaga and Noda reported the presence of $\alpha'$ and $\varepsilon$ martensite in cathodically charged 304 stainless steel following fatigue loading [6]. The presence of $\varepsilon$ martensite was attributed to the charging method whereas $\alpha'$ martensite was attributed to the fatigue loading. Furthermore, around the crack tip in 304 stainless steel, hydrogen caused a reduction in the density of slip bands and a decrease in the distance they extended from the crack tip [7]. These observations were interpreted in terms of hydrogen constraining the plastic zone [7–9]. Other effects of hydrogen have been reported. Uyama et al. [17] observed that slip on the surface of a ferritic steel changed with environment: when fatigued in air, slip bands on the surface of the sample covered the ferritic grain (parallel slip or cross-slip) whereas in the presence of hydrogen, discrete slip bands forming a "zebra pattern" were present in 50% of the grains. This change was attributed to hydrogen enhancing slip, which, in conjunction with cyclic loading, localized slip to preferred systems and created the bands. Cai and McEvily [18] observed an elongated cell structure beneath fatigue "striation-like" markings in 1018 steel tested in air. The cell width in the direction of the fatigue crack propagation matched the distance between the markings.

Although instrumentation and technique advances have enhanced our understanding of the fatigue processes, the fundamental deformation mechanisms and processes responsible for creating the surfaces and the detailed features on them are generally determined by *a posteriori* analysis, deduction using knowledge about processes that might occur, but with experimental verification being rare. The introduction of the focused ion beam, FIB, instrument has provided the capability to extract samples normal to the fracture surface such that the microstructure immediately beneath it can be examined in the transmission electron microscope. Several recent applications of this method have

* Corresponding author at: Dept. of Materials Science and Engineering, University of Illinois, Urbana, IL 61801, United States. Tel.: +1 217 333 6776; fax: +1 217 333 2736.
*E-mail address:* ianr@illinois.edu (I.M. Robertson).

0142-1123/$ - see front matter © 2012 Elsevier Ltd. All rights reserved.
http://dx.doi.org/10.1016/j.ijfatigue.2012.08.009

**Table 1**
Chemical composition of 304 and 316 stainless steels.

| | C (mass %) | Si (mass %) | Mn (mass %) | P (mass %) | S (mass %) | Ni (mass %) | Cr (mass %) | Mo (mass %) | H (mass ppm) |
|---|---|---|---|---|---|---|---|---|---|
| 304 | 0.056 | 0.43 | 1.72 | 0.03 | 0.025 | 8.87 | 18.26 | 0.22 | 2.2 |
| 316 | 0.045 | 0.3 | 1.36 | 0.026 | 0.029 | 9.91 | 17 | 2.05 | 3.4 |

revealed a complex and unexpected microstructure immediately beneath the hydrogen-induced fracture surface in different metals tested under different conditions [19–22]. These observations and the resulting correlation with the fracture surface morphologies illustrate the difficulty of predicting the underlying dislocation structure, and hence the deformation processes, from fracture surface morphologies alone.

In this paper, FIB machining is used to extract specimens normal to the primary features of fatigue fracture surfaces of samples of 304 and 316 stainless steel both in the presence and in the absence of hydrogen. The objective is to reveal the evolved microstructure in hydrogen-charged and uncharged 304 and 316 stainless steels that had been subjected to fully-reversed fatigue loading; the tests were performed in air, with the exception of 304 uncharged stainless steel, which was tested in a gaseous hydrogen environment at 10 MPa as well as in air. This paper focuses on the microstructure evolution during the fatigue testing, leaving the correlation of the microstructure with the fatigue properties until later.

## 2. Experimental procedure

Fatigue tests were performed at HYDROGENIUS at Kyushu University, Fukuoka, Japan. Samples were of a tensile bar design with a diameter of 7 mm and a gage length, which was polished to a mirror finish, of 30 mm. A hole with diameter of 100 μm and a depth of 100 μm was drilled in the middle of the gage length to act as a crack initiation site. This geometry was chosen to facilitate a study of small crack propagation; see Murakami et al. for details [7].

For purposes of comparison, 304 and 316 stainless steels (compositions in Table 1) were selected for this study. The monotonic yield strengths are 309 MPa and 271 MPa for the 304 and 316 stainless steels, respectively. To determine the effect of hydrogen on the fatigue microstructure, samples were tested either in air in the charged and in the uncharged condition, or in a high pressure (10 MPa) gaseous hydrogen environment. The latter tests were conducted on 304 stainless steel only and, using the expression $C_L = Kf^{1/2}$, where $C_L$ is the lattice concentration of hydrogen, $K$ is the room temperature solubility of the steel, and $f$ is the fugacity, which is approximately equal to the pressure ($P$) under these conditions, the equilibrium concentration of hydrogen was calculated to be approximately 10 wt. ppm [23]. The 316 stainless steel was pre-charged in a 10 MPa gaseous $H_2$ atmosphere at 270 °C for 400 h, giving a lattice concentration, as determined by thermal desorption spectroscopy, of approximately 10 wt. ppm.

All samples were fatigued under the same conditions with a fully reversed applied load ($R = -1$) of 280 MPa at a frequency of 1 Hz. All samples, other than the 304 stainless steel tests that were conducted in a hydrogen environment, were fatigued under ambient conditions. Previous studies have shown that for the pre-charged samples, the hydrogen loss during the fatigue test is insignificant [7]. Furthermore, given the level of hydrogen in these samples, the contribution of hydrogen from a moist environment is not considered to be significant [16,24].

Fracture surfaces were examined in both a JEOL 6060LV scanning electron microscope (SEM) and a FEI 235 Dual-Beam Focused Ion Beam (FIB) microscope operated in electron mode at 10–15 kV. To examine the microstructure immediately beneath the fracture surface, transmission electron microscopy (TEM) samples were extracted from specific locations on the fracture surface using the FIB lift-out technique. The FEI 235 FIB was used for the fracture surface extractions, while samples were extracted from polished round bar surfaces by using an FEI Helios Nanolab600 FIB. Examples of the sample geometry are shown in Fig. 1. The FIB fractographs, Fig. 1a and b, show the positioning of the platinum strip perpendicular and parallel to striations; other samples were extracted from flat surfaces. The platinum layer and the fracture surface of the region to be examined are shown in the FIB image presented in Fig. 1c; the trenches on either side of the protected volume are evident. To lift-out the sample, a u-cut is made, the lift-out needle attached and the final cuts made to release the sample; the approximate position of the u-cut is indicated schematically in Fig. 1c. An example of the final electron transparent sample is shown in Fig. 1d. The fracture surface as well as the platinum layer can be seen. As in previous studies [19–21], this micrograph shows the fracture surface is preserved during the FIB lift-out process, as is the underlying microstructure. To determine how the microstructure was evolving ahead of the advancing crack, samples were extracted from the free surfaces of fatigue tests interrupted after 8000 cycles at a distance of approximately 1 μm ahead of the crack tip. All samples were examined in a JEOL 2010 $LaB_6$ TEM operated at 200 kV.

## 3. Results

SEM examination showed that the fracture surface was comprised predominantly of striations. Fractographs, acquired approximately the same distance from the crack origin, from the uncharged and hydrogen-charged steels are compared in Fig. 2. Fig. 2a and b compare the striations produced in the uncharged 304 stainless steel tested in air and in a gaseous hydrogen environment, respectively. Fig. 2c and d compare the striations existing on the fracture surfaces of uncharged and hydrogen-charged 316 stainless steel, respectively. From a simple visual inspection, it is obvious that the test environment influences the striations in both steels, with the distance between striations as well as the striation height decreasing when hydrogen was present either in internal or external form. Quantitatively, the striation spacing decreased from 1 μm to 300 nm in 304 stainless steel and from 3 μm to 700 nm in 316 stainless steel due to the presence of hydrogen. The striation height on 304 stainless steel could be up to 200 nm in uncharged material compared to ~50 nm in the presence of hydrogen. In 316 stainless steel, the striation height decreased from 175 nm to 80 nm due to solute hydrogen. Other differences attributable to the presence of hydrogen, but not shown, include the overall roughness of the fracture surface. In uncharged samples, the fracture surface was more uniformly flat with different areas of striations at approximately the same height, whereas, in the presence of hydrogen, steps a micrometer or more in height separated different sets of striations. Furthermore, two other features were more common in the presence of hydrogen: rough areas without distinguishable striation features and flat features with barely perceptible striation bands. This latter feature might suggest that rubbing during closure is greater in the presence of hydrogen and this, in turn, generates the flatter surface with less distinct features or be indicative of failure along an interface such as a martensitic

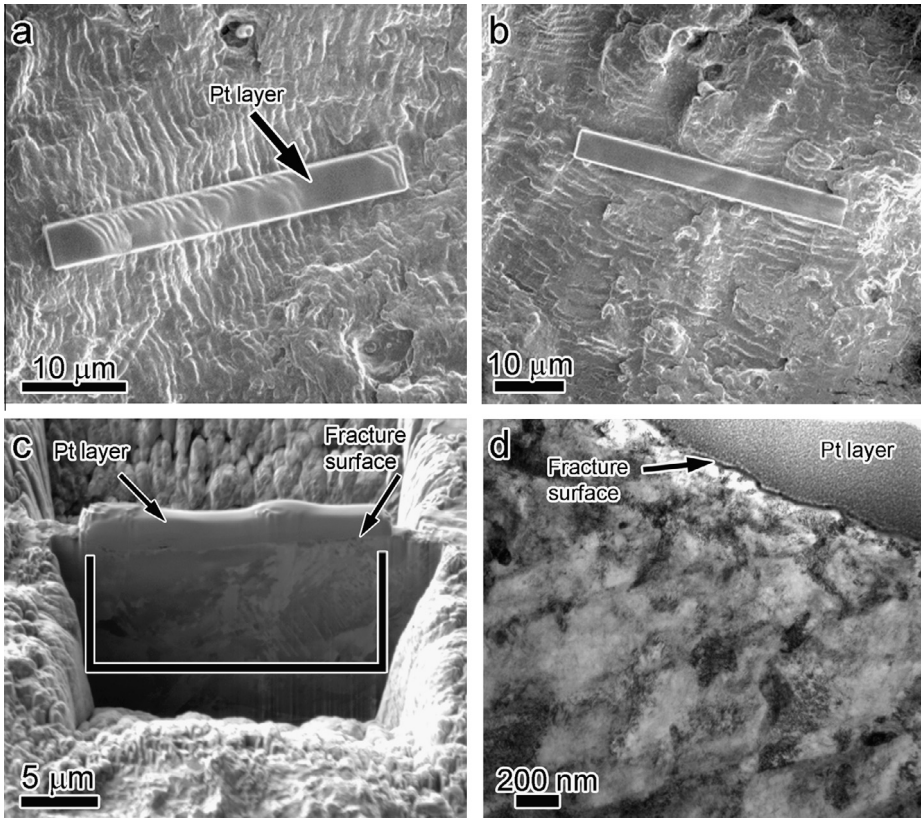


**Fig. 1.** FIB fractographs showing the orientation of the deposited platinum strip, and the corresponding sample. (a) Platinum strip deposited perpendicular to striations. (b) Platinum strip deposited parallel to striations. (c) FIB micrograph showing side view of sample prior to extraction from surface. Highlighted region indicates the approximate position of the u-cut, which defines the volume to be extracted. (d) TEM micrograph showing preserved fracture surface beneath platinum layer.

interface or a twin boundary [15,16]. If these features were attributable to rubbing contact, the microstructure beneath the fracture surface would be different from under striations.

In the case of 304 stainless steel tested in a high-pressure gaseous hydrogen environment, the microstructure beneath the striations evolves with distance from the fracture surface. As shown in the bright-field micrographs presented in Fig. 3, immediately beneath the striations, there exists a layer 0.5–1 μm thick of irregularly shaped sub-grains with dimensions between 50 and 200 nm, which is a significant reduction from the original grain size of 15 μm, Fig. 3c. The diffraction pattern from this area, Fig. 3c inset, shows splitting of the diffraction spots. This indicates the misorientation between adjacent sub-grains is a few degrees. Occasionally, as evident in Fig. 3b, immediately below the fracture surface, shear bands are seen to extend directly from the fracture surface, through the layer of refined grains, to a depth of at least 15 μm; this depth is set by the size of the extracted sample and does not suggest that this microstructure terminates at this distance. Dislocations, but not other phases, exist within these bands.

Beneath the layer of sub-grains, and extending through the depth of the FIB sample (10–15 μm in depth), is a microstructure consisting of planar features and dislocations, see Fig. 3a and d. Analysis of selected area diffraction patterns revealed the presence of a BCC structure within a FCC matrix, which is consistent with the planar features being laths of strain-induced $\alpha'$ martensite, Fig. 4b. The laths are approximately 100 nm-wide with an inter-lath spacing on the order of 100–500 nm. As shown in the micrographs presented in Fig. 4a and b, which was from a sample extracted perpendicular to the striations, several intersecting martensite lath variants coexist. At lath variant intersections, one variant is displaced suggesting that they formed sequentially with the last formed cutting through and displacing the others. The martensite laths appear to line up with the surface striations, but the surface layer of refined grains interrupts the intersection and prevents a direct correlation. The microstructure of samples extracted parallel to striations, as shown in Fig. 4c, was similar to that in samples extracted perpendicular to the striations, although more variants of martensite were apparent in the perpendicular slices.

In uncharged 304 stainless steel fatigued under ambient conditions, the microstructure is again refined but to a significantly lesser extent than when the tests are conducted in a high-pressure gaseous hydrogen environment. The resulting microstructure, as shown in the micrographs presented in Fig. 5, consists of elongated grains with a diameter of ~500 nm and extends at least 10–15 μm from the fracture surface; again, the depth is set by the size of the extracted sample, and should not be interpreted as indicating that the microstructure ends at this depth. A similar microstructure exists in samples extracted parallel to the striations. Analysis of selected area diffraction patterns, Fig. 5c–e, confirms that these grains have a predominantly BCC structure with only a few exhibiting an FCC structure. That is, much of the volume beneath the fracture surface and extending 10–15 μm from it has been transformed to martensite, which is in marked contrast to the evolved microstructure produced when tests were conducted in a gaseous hydrogen environment. As in the case of 304 stainless steel deformed in a gaseous hydrogen environment, there was no obvious correlation between the refined microstructure and the features on the fracture surface, as shown in Fig. 5b.

The depth dependence of the evolved microstructures beneath the fracture surface of hydrogen-charged 316 stainless steel is presented in the electron micrographs of Fig. 6. This microstructure consists of a refined sub-grain structure with grains 100–200 nm

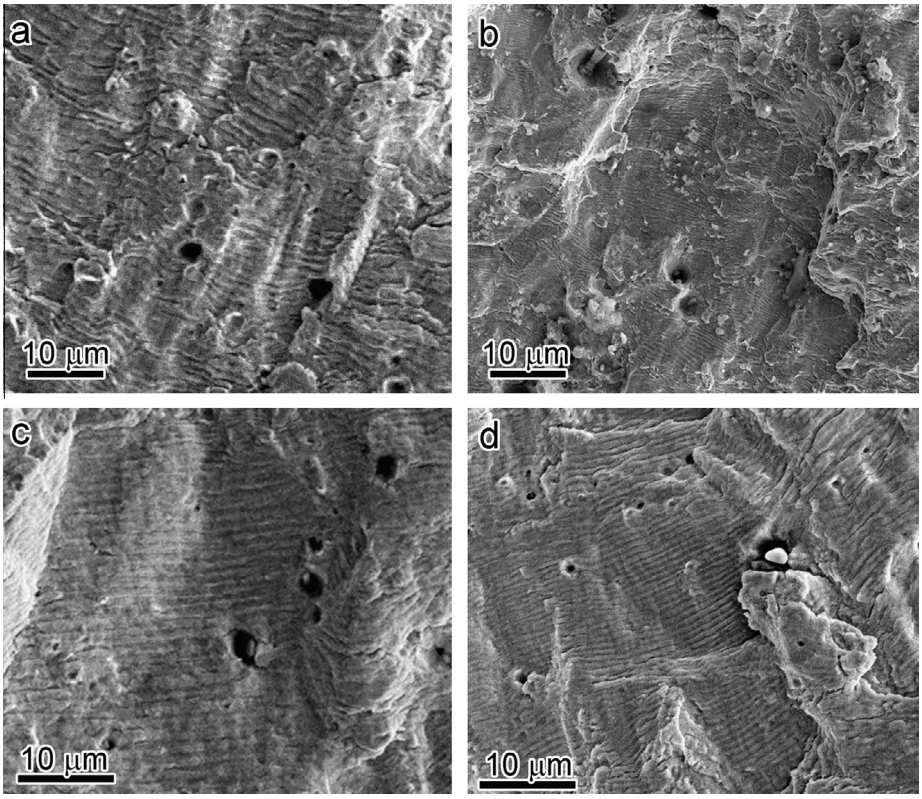


**Fig. 2.** SEM fractographs comparing fatigue striations formed under different conditions. (a) Uncharged 304 stainless steel fatigued under ambient conditions; (b) uncharged 304 stainless steel fatigued in 10 MPa gaseous hydrogen environment; (c) uncharged 316 stainless steel fatigued under ambient conditions; and (d) hydrogen-charged 316 stainless steel, 10 wt. ppm hydrogen, and fatigued under ambient conditions.

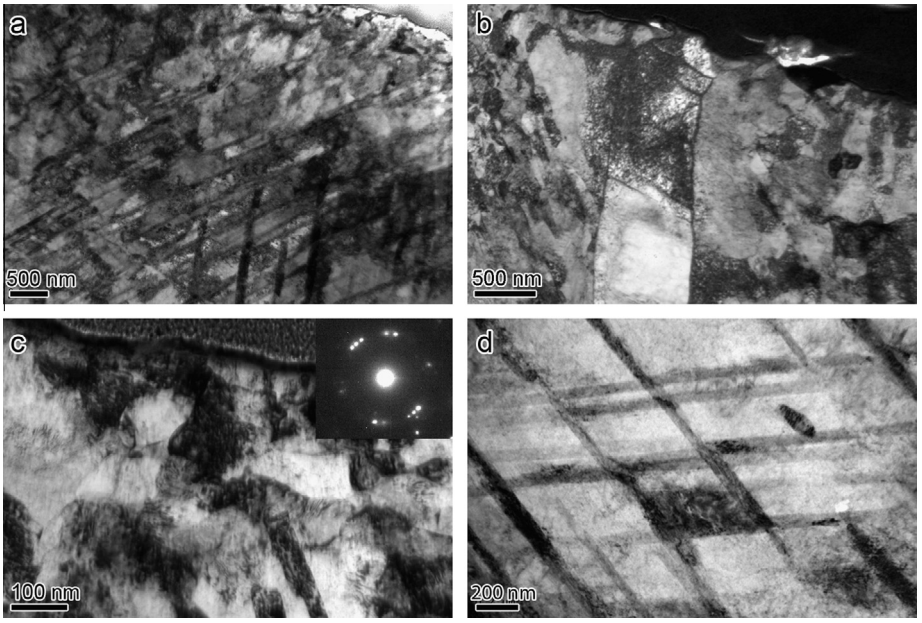


**Fig. 3.** TEM micrographs showing microstructure immediately beneath striations of 304 stainless steel fatigued in a 10 MPa gaseous hydrogen environment. (a) Overview of microstructure showing fracture surface in upper right corner. (b) Shear band extending from fracture surface. (c) Fine grain structure immediately beneath fracture surface. Inset shows diffraction pattern (⟨1 1 1⟩ zone axis) taken from area showing splitting of spots due to small rotations between grains. (d) Martensite laths approximately 5 μm from fracture surface.

in diameter existing to a depth of 1 μm beneath the fracture surface, Fig. 6a. Again, this is a significant decrease from the original grain size of 13 μm. It is also consistent with the effect of a gaseous hydrogen environment on the microstructure immediately beneath striations in 304 stainless steel; compare the micrographs presented in Figs. 3 and 6. With increasing distance from the fracture surface, the microstructure transitions from a refined subgrain structure to one consisting of dislocations and planar features

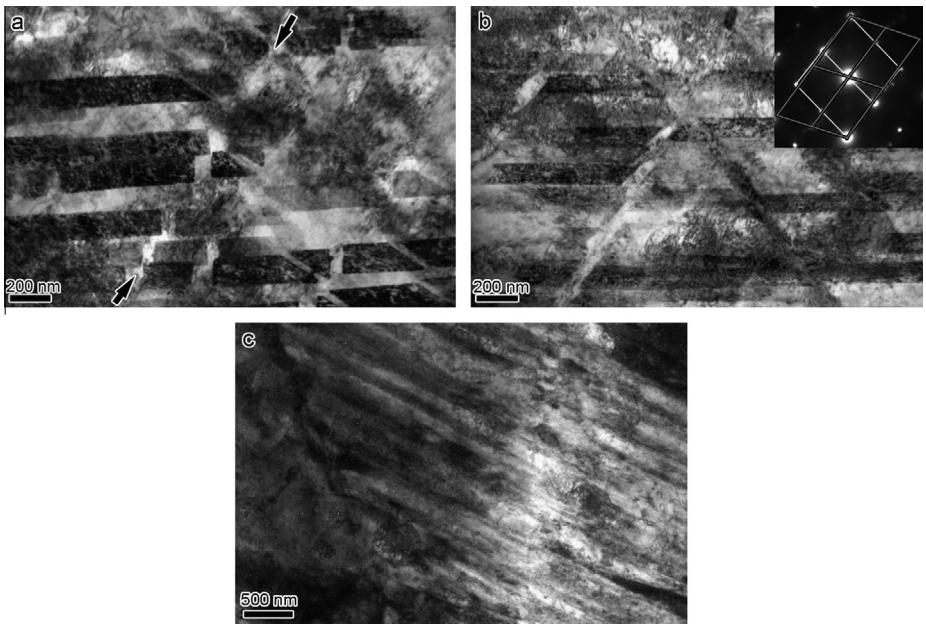


**Fig. 4.** TEM micrographs showing martensite laths in 304 stainless steel fatigued in hydrogen atmosphere approximately 5 μm from fracture surface. (a) TEM micrograph showing laths in sample taken perpendicular to striations. One set of laths is in contrast (black), while the other two are out of contrast (light). However, the intersections are evident, and the two light sets have clearly been displaced by the other variant. An example lath is marked by arrows. (b) TEM micrograph of same area as (a) but at a different sample tilt. Inset is a diffraction pattern of the area showing a BCC ⟨1 2 3⟩ pattern (white) overlaid on FCC ⟨0 1 3⟩ (gray). (c) TEM micrograph showing laths in sample taken parallel to striations. Note that only one set of parallel laths is visible.

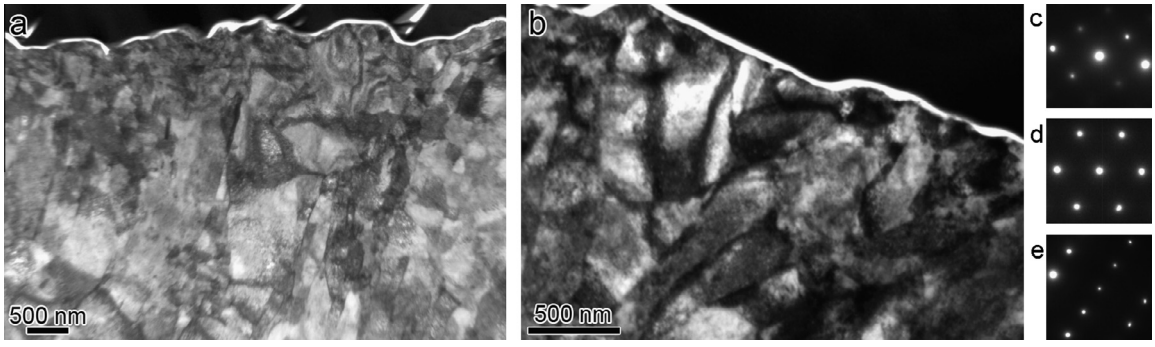


**Fig. 5.** (a) TEM micrograph showing microstructure beneath striations of 304 stainless steel fatigued under ambient conditions. (b) Fine grains immediately beneath fracture surface. (c–e) Diffraction patterns taken of same area at different tilts showing BCC (c) ⟨0 0 1⟩, (d) ⟨1 1 1⟩, and (e) ⟨1 1 3⟩ zone axis.

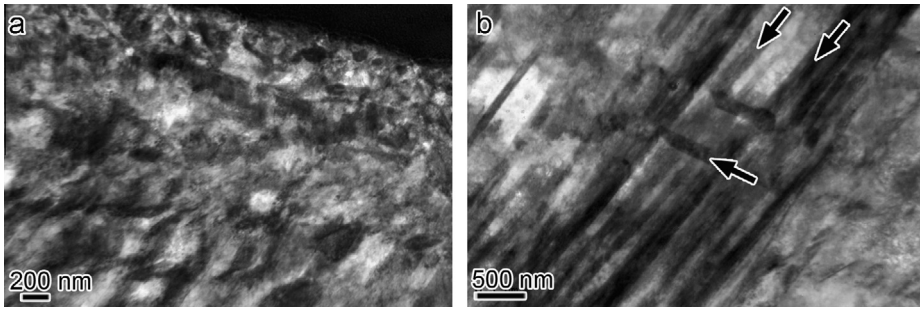


**Fig. 6.** TEM micrographs showing microstructure beneath striations of 316 stainless steel precharged with hydrogen and fatigued in atmosphere. (a) Fine grains immediately beneath fracture surface. (b) Planar features extending approximately 5 μm beneath fracture surface, examples indicated by arrows.

that lie perpendicular and parallel to the fracture surface. An example of this microstructure is shown in the micrograph presented in Fig. 6b; examples of the planar features are indicated by arrows. As can be seen from the micrograph, the planar features perpendicular to the fracture surface appear to be closer spaced than those parallel to it. Diffraction pattern analysis revealed austenite, suggesting that these planar features are not martensite. They may be twins or overlapping stacking faults, but this remains to be confirmed by electron diffraction. The lack of martensite in the hydrogen-charged 316 stainless steel is expected and is in marked

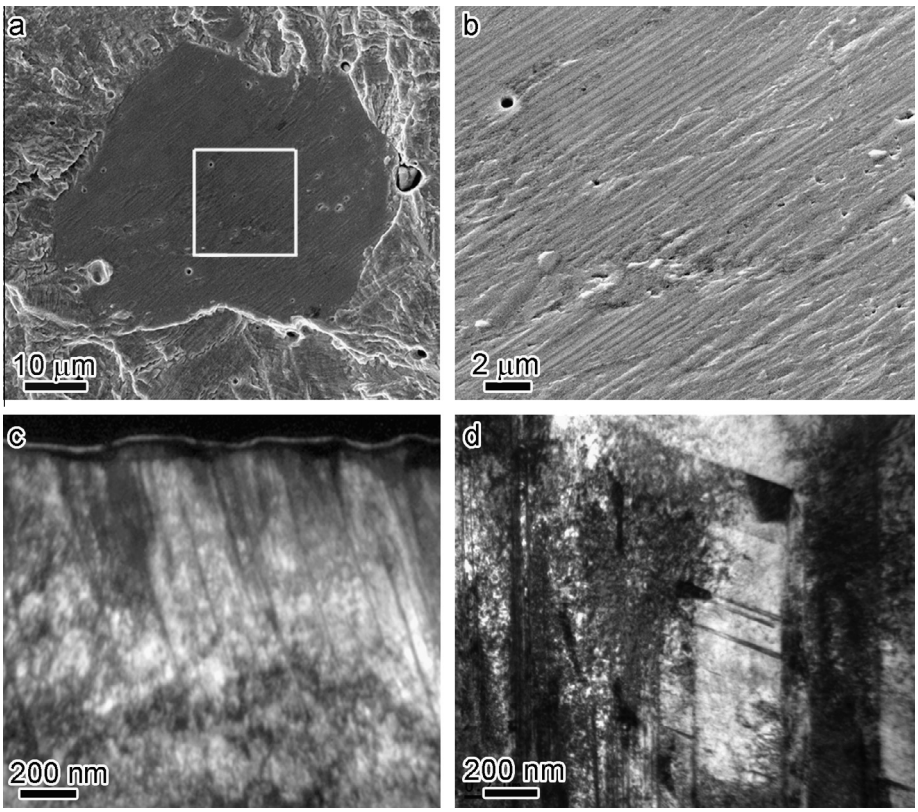


**Fig. 7.** (a) SEM fractograph of flat fracture feature of 316 stainless steel precharged with hydrogen. (b) Higher magnification of the flat fracture surface showing fine striations. (c) TEM micrograph showing microstructure immediately beneath flat feature. (d) TEM micrograph with closer view showing fine features perpendicular to planar features seen in (c).

contrast to the evolved microstructure in 304 stainless steel tested in a gaseous hydrogen environment.

Preliminary results, not presented, of the microstructure beneath fatigue striations formed in uncharged 316 stainless steel fatigued in air revealed that it is different than that produced in the presence of hydrogen and, also, different than that produced in 304 stainless steel deformed in the presence and absence of hydrogen. Again, there is a refinement in the microstructure immediately beneath the fracture surface. However, immediately beneath and extending a distance of between 400 and 600 nm the refinement takes the form of a banded structure with the bands tending to lie parallel to the fracture surface. The inter-band spacing is 50–100 nm and between the bands exist dislocations cells and dislocations. This microstructure is strikingly similar to that produced by compressive loading or rolling to high strains [25]. Further from the fracture surface, these bands exist but now lie inclined to the fracture surface. Between the bands dislocation cells (2 μm in size) form a mosaic pattern and there also exists deformation twins. This structure extends for more than 7 μm from the surface (depth limit is due to sample size, and is not an indication that the evolved microstructure ends at this depth). Details of the misorientation between the bands and the cell structures remain to be determined.

In addition to regions exhibiting striation markings, other regions on the fracture surface of hydrogen precharged 316 stainless steel appeared relatively flat at low magnification. An example of such a region is shown in the fractograph presented in Fig. 7a. At higher resolution, it is seen that such surfaces are covered with fine striation markings; compare Fig. 7b, which is the boxed area in Fig. 7a at higher magnification, with Fig. 2d. This structure may reflect surface-to-surface contact and rubbing during the compressive portion of the cycle or an alternate fracture path that may involve interfaces or grain boundaries. To determine the underlying microstructure, samples were cut from the surface perpendicular to the markings such that several would be evident in an electron micrograph. As shown in the bright-field images presented in Fig. 7c and d, the microstructure beneath the surface consists of a high density of dislocations interspersed with fine planar features that extend 2 μm from the surface. Examination of the cross-section of the fracture surface, top of Fig. 7c, shows it is not flat but contains undulations that are approximately 50 nm in height and irregularly spaced. These correspond to the fine striation markings seen in the fractograph presented in Fig. 7b. In comparison with the underlying microstructure, it is seen that the planar features appear related to the undulations, although the correspondence is not one-to-one as more planar features than undulations exist, see Fig. 7d, The fine planar features may be twins but this remains to be confirmed by electron diffraction. This microstructure, while also produced in hydrogen, is significantly different from the microstructure beneath the hydrogen-induced striations.

Finally, to understand the chronology of how the microstructure evolves in the hydrogen-charged material during the fatigue cycles, FIB samples were extracted from the polished surface 1 μm and ~5 μm ahead of arrested cracks from fatigue tests interrupted after 8000 cycles. An example of the resulting microstructure in 304 stainless steel is shown in the micrographs presented in Fig. 8. Fig. 8a shows the relationship of the extracted sample (Pt strip) to the arrested crack and the resulting microstructure is shown in Fig. 8b. Within ~1 μm of the crack, planar features (martensite plates) coexist with dislocations although there are regions in which only dislocations exist. The microstructure approximately 5 μm ahead of the crack tip consists of dislocations only. The

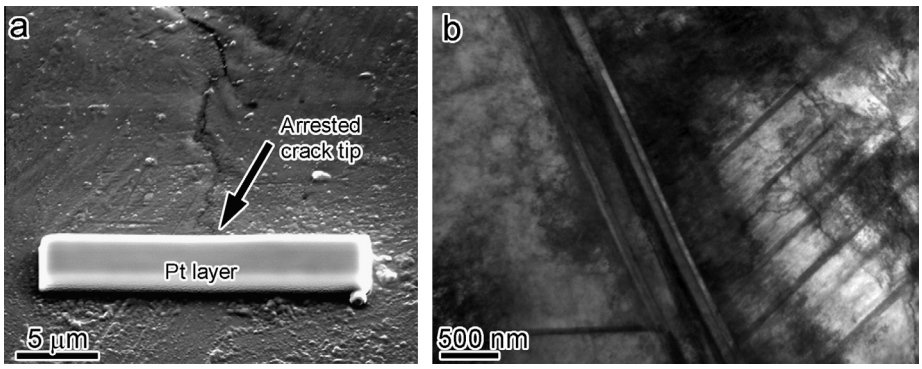


**Fig. 8.** (a) FIB image showing location of Pt strip ahead of crack tip of 304 stainless steel tested in hydrogen; this indicates the location from which the sample was extracted. (b) TEM micrograph showing microstructure immediately ahead of crack tip. Right region shows example of martensite laths, while left region shows area with just dislocation activity.

microstructure ahead of an arrested crack in 316 stainless steel showed a similar dependence on distance from the crack, although the planar features were not martensite but twins.

## 4. Discussion

The microstructure evolution as a function of depth beneath fatigue striations and flat regions on the fracture surface of uncharged and hydrogen-charged 304 and 316 stainless steel have been compared. The evolved microstructure is dependent on the steel and on the presence or absence of hydrogen, although it is unclear that internal versus external hydrogen has a significant effect. The key findings related to microstructural differences can be summarized as:

1. Beneath striations in uncharged 304 stainless steel tested in a gaseous hydrogen environment, a graded microstructure with nano- and ultra-fine sub-grains extends 1 μm from the surface before transitioning to dislocations with planar martensite. With increasing distance ahead of an arrested fatigue crack, the microstructure beneath the sample surface transitioned from dislocations with martensite to predominantly dislocations.
2. Beneath striations in uncharged 304 stainless steel tested under ambient conditions, the refinement of the microstructure to ~500 nm diameter sub-grains for a distance of 10 μm beneath the fracture surface was accompanied by a transition to martensite.
3. Beneath striations in hydrogen-charged 316 stainless steel, the microstructure exhibited a band of 100–200 nm sized sub-grains and this transitioned into a region containing dislocations and planar features. The planar features were not martensitic and most likely are twins although this remains to be confirmed. With distance from an arrested fatigue crack, the microstructure beneath the sample surface transitioned from dislocations with planar features, most likely deformation twins, to predominantly dislocations.
4. Beneath flat features on fracture surfaces in hydrogen-charged 316 stainless steel, the microstructure consisted of dislocations and planar features that extended from the fracture surface into the material. The refinement seen beneath striations produced in hydrogen-charged 316 was not observed beneath the flat surfaces.
5. Beneath striations in uncharged 316 stainless steel, there exists a banded structure that lies parallel to the fracture surface. This structure transitions to a banded structure with the bands inclined to the fracture surface. Within the bands there exist dislocations which in some regions form a cell structure and deformation twins.

The microstructure beneath fatigue striations in both 304 and 316 stainless steel has been shown to be markedly different when the tests are conducted in the absence and presence of hydrogen. From the observations of the hydrogen-induced microstructure ahead of arrested fatigue cracks, the deformation mechanism is seen to be predominantly due to dislocations, although in 304 stainless steel, as the crack is approached, there is evidence for the formation of strain-induced martensite plates. The martensite plates form sequentially, as evidenced by the displacement of some plates due to the formation and extension of another variant. This microstructure, however, is different from that observed immediately beneath striations formed in 304 stainless steel in the presence of hydrogen, which contains the refined sub-grain microstructure. This raises an interesting question of what drives the transition from a microstructure of dislocations with martensite plates to a refined sub-grain structure in which there is no evidence of martensite. Here, the difference between the microstructure evolution in 304 stainless steel in the presence and absence of hydrogen is not considered, as the primary difference is related to hydrogen restricting the transformation to martensite. Similarly, in 316 stainless steel, testing in the presence of internal hydrogen results in the formation of the sub-grain layer and no deformation twinning whereas in the absence of hydrogen a banded structure exists. Several possibilities could account for the formation of the sub-grained structure immediately beneath the striations when hydrogen is present. For example, the evolved microstructure could be generated:

1. During the process of crack advance. This implies hydrogen influences the deformation processes as the microstructure immediately beneath the striations depends on the test environment. This difference is most striking in 316 stainless steel.
2. By energy minimization processes associated with the formation of low-energy dislocation structures. Again, this implies an influence of hydrogen on the evolved microstructural processes.
3. By rubbing during the closure cycle. Contact of the surfaces certainly occurs under this loading condition. Even if the microstructure beneath striations is due to rubbing the observations suggest an influence of hydrogen as the evolved form is dependent on test environment.
4. By recrystallization and recovery processes. The temperature for reversion of the $\alpha'$ martensite is 550 °C in 304 and 316 stainless steel and the recrystallization temperature is above 700 °C with complete recrystallization occurring at 1000 °C [26]. Dynamic recrystallization is expected to occur at elevated temperatures and has been reported to occur at temperatures of 900 °C.

As these tests were conducted at room temperature, the latter possibility can be excluded because at these temperatures hydrogen acts as a strengthening agent rather than a plasticity enhancer. Additional studies are needed to ascertain the contribution of each of the other possibilities; such investigations are in progress.

The hydrogen-evolved microstructure under the flat regions is different from that under the main striations with no evidence for the formation of sub-grains. Indeed, the microstructure is similar to that found in regions on the sample surface in close proximity to the arrested fatigue crack. This might indicate that such regions are generated rapidly, linking regions showing striations. One possible fast crack path could be a grain boundary or martensite lath boundary weakened by hydrogen. This possibility remains to be verified.

In the work reported herein, striation spacing and height decreased with the presence of hydrogen during loading. This result is contrary to previous findings in which the distance between striations increased in the presence of hydrogen. This result was interpreted and validated as being indicative of greater cyclic crack advance in the presence of hydrogen. Of course, the magnitude of the striation spacing depended on the distance from the fracture origin, but was always larger in the presence of hydrogen [15]. Although every effort was made to extract samples from the same distance from the crack, it is possible that variations in the spacings reflect this difference. However, assuming this is not the case, the striation spacing in the presence of hydrogen may reflect a difference in mechanism, with crack advance in ambient conditions being related to the classical mechanism and the striation spacing associated with cyclic crack advance, whereas in hydrogen, crack advance and the formation of striations may be controlled by the need to develop a critical stress first. These possibilities are currently being explored.

In 304 stainless steel the influence of hydrogen is more profound as it suppresses the wide-scale transformation to martensite. This is consistent with previous observations and has been attributed to hydrogen causing a narrowing of the plastic zone [9].

It is clear that the presence of hydrogen changes the deformation processes accompanying fatigue loading and crack advance. The enhancement of the deformation processes and acceleration of the evolved microstructure by hydrogen can be ascribed to the hydrogen-enhanced localized plasticity (HELP) mechanism [27–30]. In this mechanism, hydrogen associated with dislocations and obstacles effectively shields the interactions and reduces the interaction energy of dislocations with obstacles in specific directions. Consequently, the dislocation velocity is increased, or, alternatively, the same velocity is reached at a lower shear stress and the equilibrium distance between dislocation decreases. Previous attempts to show that the presence of hydrogen accelerated the evolution of the dislocation density or the microstructure yielded mixed results. For example, prior attempts to find differences in dislocation density and distribution in Ni were inconclusive as no statistically significant differences were found between behavior in a hydrogen versus an inert gas environment [31,32]. In contrast, Matsui et al. reported an increase in dislocation density in Fe cathodically charged at 200 K and deformed in tension [33]. More recent studies, in which the hydrogen concentration was significantly greater than in previous studies, have shown a discernible difference in the dislocation density and evolved microstructure. As an example, Martin et al. reported that the refinement of the dislocation cell structure beneath intergranular facets in nickel containing 2000 at. ppm H was typical of nickel strained to 40% and not the actual 13% strain at failure [21]. It is important to note that the dislocation structure at 40% strain may have evolved beyond dislocation cells, which would suggest that hydrogen stabilizes the structures and delays the transition. Here it is suggested that hydrogen enhances and accelerates the plastic processes in both 304 and 316 stainless steel. A consequence of this, irrespective of when and how the dislocations are generated, is that there is significant dislocation generation such that the pre-existing microstructure is destroyed and replaced with a refined sub-grain structure that extends up to 1 μm from the fracture surface. The extent of the refinement simply reflects the degree of deformation that has occurred. Future efforts will emphasize determining when these dislocations are generated, and how this microstructure relates to the fracture surface and the morphological features that exist on it.

## 5. Conclusions

The microstructure beneath fracture surface cannot be ascertained using *a posteriori* analysis methods. However, it can be revealed by using the focused ion beam lift-out technique to extract samples normal to the surface for TEM examination. A challenge remains in interpreting how this microstructure evolves and correlates with the features on the fracture surface.

Hydrogen has a profound effect on the microstructure evolution produced under fatigue loading in both 304 and 316 stainless steel. In the presence of hydrogen, a refined sub-grain structure is developed in both systems, which is distinctly different from the microstructure generated in the absence of hydrogen.

## Acknowledgements

This work was supported by DOE EERE Grant GO15045 (MLM, PS and IMR) and by NEDO (YM) Fundamental Research Project on Advanced Hydrogen Science (2006–2012). The authors gratefully acknowledge the support of the International Institute for Carbon Neutral Energy Research (WPI-I2CNER), sponsored by the World Premier International Research Center Initiative (WPI), MEXT, Japan. Microscopy was carried out in part in the Frederick Seitz Materials Research Laboratory Central Facilities, University of Illinois. MLM gratefully acknowledges the assistance of K. Nonaka at HYDROGENIUS with the fatigue testing. IMR acknowledges the support of the National Science Foundation.

## References

[1] Oriani RA. Hydrogen – the versatile embrittler. Corrosion 1987;43:390–7.
[2] Birnbaum HK, Robertson IM, Sofronis P, Teter D. Mechanisms of hydrogen related fracture – a review. In: Magnin T. editor. Corrosion deformation interactions CDI'96, second international conference, The Institute of Materials, Great Britain, Nice, France; 1997. p. 172–95.
[3] Suresh S, Ritchie RO. On the influence of environment on the load ratio dependence of fatigue thresholds in pressure vessel steel. Eng Fract Mech 1983;18:785–800.
[4] Suresh S, Ritchie RO. Mechanistic dissimilarities between environmentally influenced fatigue-crack propagation at near-threshold and higher growth rates in lower strength steels. Met Sci 1982;16:529–38.
[5] Gangloff RP, Ritchie RO. Environmental effects novel to the propagation of short fatigue cracks. In: Fundamentals of deformation and fracture. Eshelby memorial symposium. Sheffield (Engl): Cambridge Univ Press; 1985. p. 529–58.
[6] Matsunaga H, Noda H. Visualization of hydrogen diffusion in a hydrogen-enhanced fatigue crack growth in type 304 stainless steel. Metall Mater Trans A 2011;42:2696–705.
[7] Murakami Y, Kanezaki T, Mine Y. Hydrogen effect against hydrogen embrittlement. Metall Mater Trans A 2010;41:2548–62.
[8] Murakami Y, Kanezaki T, Mine Y, Matsuoka S. Hydrogen embrittlement mechanism in fatigue of austenitic stainless steels. Metall Mater Trans A 2008;39A:1327–39.
[9] Murakami Y, Matsuoka S. Effect of hydrogen on fatigue crack growth of metals. Eng Fract Mech 2010;77:1926–40.
[10] Murakami Y, Takahashi K, Kusumoto R. Threshold and growth mechanism of fatigue cracks under mode II and III loadings. Fatigue Fract Eng Mater Struct 2003;26:523–31.
[11] Nibur KA, Marchi CS, Somerday BP. Fracture and fatigue tolerant steel pressure vessels for gaseous hydrogen. In: ASME 2010 pressure vessels and piping

division/K-PVP conference, PVP2010, July 18, 2010–July 22, 2010. Bellevue (WA, United States): American Society of Mechanical Engineers. p. 949–58.
[12] Darcis PP, McColskey JD, Lasseigne AN, Siewert TA. Hydrogen effects on fatigue crack growth rate in high strength pipeline steel. In: 2008 International hydrogen conference – effects of hydrogen on materials, September 7, 2008–September 10, 2008. Jackson (WY, United States): ASM International; 2009. p. 381–8.
[13] Skipper C, Leisk G, Saigal A, Matson D, Marchi CS. Effect of internal hydrogen on fatigue strength of type 316 stainless steel. In: 2008 International hydrogen conference – effects of hydrogen on materials, September 7, 2008–September 10, 2008. Jackson (WY, United States): ASM International; 2009. p. 139–46.
[14] San Marchi C, Somerday BP, Nibur KA, Stalheim DG, Boggess T, Jansto S. Fracture and fatigue of commercial grade API pipeline steels in gaseous hydrogen. In: ASME 2010 pressure vessels & piping division/K-PVP conference. Bellevue (Washington): ASME; 2010.
[15] Aoki Y, Kawamoto K, Oda Y, Noguchi H, Higashida K. Fatigue characteristics of a type 304 austenitic stainless steel in hydrogen gas environment. Int J Fatigue 2005;133:277–88.
[16] Schuster G, Altstetter C. Fatigue of stainless steel in hydrogen. Metall Mater Trans A 1983;14:2085–90.
[17] Uyama H, Nakashima M, Morishige K, Mine Y, Murakami Y. Effects of hydrogen charge on microscopic fatigue behaviour of annealed carbon steels. Fatigue Fract Eng Mater Struct 2006;29:1066–74.
[18] Cai H, McEvily AJ. On striations and fatigue crack growth in 1018 steel. In: Cyclic deformation and fatigue of solids: an international symposium in honour of Professor Campbell Laird, 11–14 March 2000. Switzerland: Elsevier; 2001. p. 86–9.
[19] Martin ML, Fenske JA, Liu GS, Sofronis P, Robertson IM. On the formation and nature of quasi-cleavage fracture surfaces in hydrogen embrittled steels. Acta Mater 2011;59:1601–6.
[20] Martin ML, Robertson IM, Sofronis P. Interpreting hydrogen-induced fracture surfaces in terms of deformation processes: a new approach. Acta Mater 2011;59:3680–7.
[21] Martin ML, Somerday BP, Ritchie RO, Sofronis P, Robertson IM. Hydrogen-induced intergranular failure in nickel revisited. Acta Mater 2012;60:2739–45.
[22] Ro Y, Agnew SR, Gangloff RP. Effect of environment on fatigue crack wake dislocation structure in Al–Cu–Mg. Metall Mater Trans A 2012;43:2275–92.
[23] Marchi CS, Somerday BP, Robinson SL. Permeability, solubility and diffusivity of hydrogen isotopes in stainless steels at high gas pressures. Int J Hydrogen Energy 2007;32:100–16.
[24] Andriamiharisoa H, Habashi M, Talbot-Besnard S, Galland J, Azou P. Effects of internal and environmental hydrogen on fatigue crack growth rate in metastable austenitic structure. In: Hydrogen effects in metals: proceedings of the 3rd international conference on effect of hydrogen on behavior of materials. Moran (WY, USA): Metall Society of AIME; 1981. p. 619–28.
[25] Hughes DA, Hansen N. Deformation structures developing on fine scales. Philos Mag 2003;83:3871–93.
[26] Herrera C, Plaut RL, Padilha AF. Microstructural refinement during annealing of plastically deformed austenitic stainless steels. Mater Sci Forum 2007;550:423–8.
[27] Robertson IM. The effect of hydrogen on dislocation dynamics. Eng Fract Mech 2001;68:671–92.
[28] Birnbaum HK, Sofronis P. Hydrogen-enhanced localized plasticity – a mechanism for hydrogen-related fracture. Mater Sci Eng A, Struct Mater, Prop Microstruct Process 1993;A176:191–202.
[29] Liang Y, Sofronis P, Aravas N. On the effect of hydrogen on plastic instabilities in metals. Acta Mater 2003;51:2717–30.
[30] Lufrano J, Sofronis P. Numerical analysis of the interaction of solute hydrogen atoms with the stress field of a crack. Int J Solids Struct 1996;33:1709–23.
[31] Robertson IM, Birnbaum HK. Effect of hydrogen on the dislocation structure of deformed nickel. Scripta Metall 1984;18:269–74.
[32] McInteer WA, Thompson AW, Bernstein IM. The effect of hydrogen on the slip character of nickel. Acta Metall 1980;28:887–94.
[33] Matsui H, Kimura H, Kimura A. The effect of hydrogen on the mechanical properties of high purity iron. III. The dependence of softening on specimen size and charging current density. Mater Sci Eng 1979;40:227–34.